The Structure of $Co(\eta\text{-}C_5H_5)_2^+$ and NMe_4^+ Intercalates of $MnPS_3$: An X-ray, Neutron-Diffraction, and Solid-State NMR Study

J. S. O. Evans,† D. O'Hare,*,† and R. Clement‡

Contribution from the Inorganic Chemistry Laboratory, Oxford University, South Parks Road, Oxford, OX1 3QR, UK, and the Laboratoire de Spectrochimie des Eléments Transition, CNRS, Université Paris-Sud, 91405 Orsay, France

Received September 7, 1994®

Abstract: This paper reports a series of structural studies on the intercalation compounds of $MnPS_3$, with the aim of trying to understand the source of the magnetic and NLO properties they exhibit. Both neutron and X-ray powder experiments and single crystal studies have been performed on $Mn_{1-x}PS_3\{G\}_{2x}(H_2O)_y$ for $G = Co(\eta\text{-}C_5H_5)_2^+$ [$x = 0.34$, $y = 0.3$] and $N(CH_3)_4^+$ [$x = 0.32$, $y = 0.9$]. These investigations have suggested that the individual host layers of these intercalates contain an ordered arrangement of metal vacancies, giving rise to large superlattices in the *ab* plane of the crystal; it is this vacancy arrangement which is believed to give rise to the changes observed in the magnetic properties of these systems on intercalation. In the case of the $Co(\eta\text{-}C_5H_5)_2^+$ intercalate, the degenerate ways of layer stacking lead to a considerably disordered overall structure such that the 3-dimensional diffraction of this intercalate can be described by a considerably smaller overall unit cell than the pristine host lattice. These layer shifts also lead to a 3-layer repeat structure and a change in symmetry of the host lattice from $C2/m$ to $R\bar{3}m$. The overall diffraction pattern can then be described by a cell of dimensions $a = b = 3.532(3)$ Å, $c = 35.57(2)$ Å, $\gamma = 120°$. ^2H solid-state NMR experiments have been used to investigate the orientational preferences and dynamic properties of the cobaltocene guest molecules; these have shown a static arrangement of guest molecules at room temperature lying with their principal molecular axes parallel to the host lattice layers. As the temperature is increased the molecules begin to rotate around their C_2 axis. The tetramethylammonium intercalate appears to be considerably more ordered than the cobaltocenium intercalate, suggesting the existence of a guest superlattice in addition to the metal vacancy superlattice. The overall structure is then best explained by a hexagonal metal vacancy lattice of dimension $a = 10.6$ Å, and a guest lattice of dimensions 18.3×6.1 Å. The combination of these two cells leads to an overall hexagonal cell of dimensions $a = b = 36.6$ Å. This suggests that the overall structure of these materials can only be fully explained by adopting a unit cell with the formula $Mn_{60}P_{72}S_{216}\{Guest\}_{12}$.

Introduction

The transition metal hexathiohypodiphosphates, $M_2P_2S_6$, were first reported by Friedel in 1894, and extensively studied in the late 1960's and early 1970's by Hahn and Klingen.[1-3] They form a class of layered materials which are, to a first approximation, very similar to the transition metal dichalcogenides and, as such, were shown in the 1970's to undergo a similar range of intercalation reactions.[4,5] The first indication that these compounds exhibit a chemistry which is unique to this particular lattice, and one of the most unusual reactions of intercalation chemistry, came in 1980 when Clement reported that $MnPS_3$ would react spontaneously with aqueous solutions of ionic salts, G^+X^- (where G can range from simple ionic species such as K^+ and NH_4^+ to species as large as, for example, cobaltocenium cations), to give compounds of general formula $Mn_{1-x}PS_3\{G\}_{2x}(H_2O)_y$.[6-10] In these compounds, charge balance has been maintained by the loss of one Mn^{2+} ion from the *intra*layer region for every two G^+ ions that are adopted in the *inter*layer region.

There are a number of reasons why these compounds are of particular interest to the intercalation chemist. Firstly, this unique ion-exchange intercalation route means that intercalation reactions are no longer limited to small, highly electropositive guest species, as is the case for the transition metal dichalcogenides, but become possible for a large range of charged species. This means that molecules with potentially interesting catalytic, conducting, or optical properties can be included between the layers of an inorganic lattice, where the influence of the sterically restraining host layers may dramatically influence their properties. For example, there have been a number of recent reports in which the intercalation of cationic chromophores such as $DAMS^+$ (DAMS = (dimethylamino)-*N*-methylstilbazonium) have given rise to materials with efficient second harmonic generation.[11,12] Thus, despite the fact that pristine $MnPS_3$ crystallizes in the centrosymmetric space group

* Author to whom correspondence should be addressed.
† Inorganic Chemistry Laboratory, Oxford University.
‡ Laboratoire de Spectrochimie des Eléments Transition, Université Paris-Sud.
® Abstract published in *Advance ACS Abstracts,* March 1, 1995.

(1) Friedel, C. *C. R. Acad. Sci. Paris* **1894**, *119*, 260.
(2) Hahn, H.; Klingen, W. *Naturwissenshaften* **1965**, *52*, 494.
(3) Klingen, W.; Ott, R.; Hahn, H. *Z. Anorg. Allg. Chem.* **1973**, *396*, 271.
(4) Clement, R.; Green, M. L. H. *J. Chem. Soc., Dalton Trans.* **1979**, 1566.
(5) Johnson, J. W. In *Intercalation Chemistry*; Whittingham, M. S., Jacobson, A. J., Eds.; Academic Press: New York, 1982; p 267.
(6) Clement, R.; Girerd, J. J.; Morgenstern Badarau, I. *Inorg. Chem.* **1980**, *19*, 2852.
(7) Clement, R. *J. Chem. Soc., Chem. Commun.* **1980**, 647.
(8) Audiere, J. P.; Clement, R.; Mathey, Y.; Mazieres, C. *Physica B* **1980**, *99*, 133.
(9) Clement, R.; Garnier, O.; Jegoudez, J. *Inorg. Chem.* **1986**, *125*, 1404.
(10) Clement, R.; Doeuff, M.; Gledel, C. *J. Chim. Phys.* **1988**, *85*, 1053.
(11) Lacroix, P. G.; Lemarinier, A. V.; Clement, R.; Nakatani, K.; Delaire, J. A. *J. Mater. Chem.* **1993**, 499.
(12) Lacroix, P. G.; Clement, R.; Nakatami, K.; Zyss, J.; Ledaux, I. *Science* **1994**, *263*, 658.

0002-7863/95/1517-4595$09.00/0

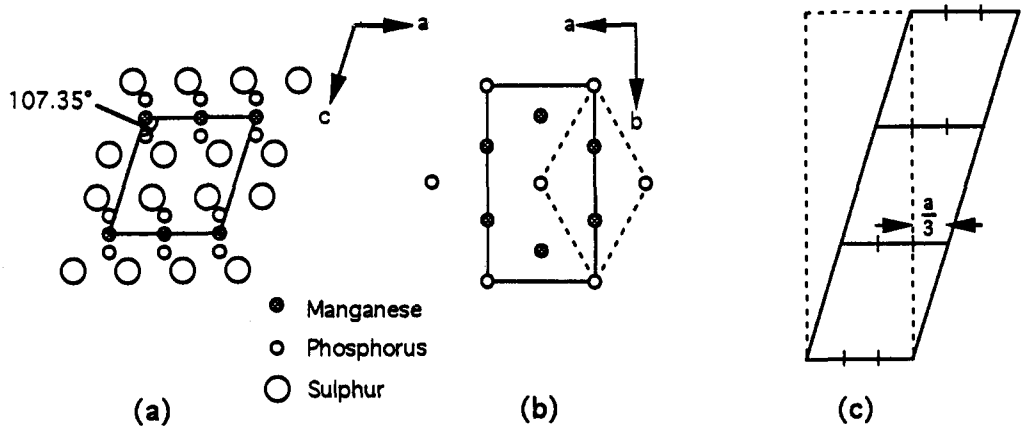

Figure 1. The unit cell of $MnPS_3$. (a) A view of the *ac* plane, showing the monoclinic angle of 107.35°. (b) A view of the *ab* plane with the monoclinic cell shown with a solid line and the related hexagonal cell shown with a dashed line. (c) A view of the *ac* plane showing how the monoclinic cell is related to the hexagonal cell by a tripling of the *c* axis.

C2/m, the active guest molecules pack with the lack of symmetry requisite for non-linear optical activity to be observed. Secondly, whilst the pristine host lattice $MnPS_3$ is a two-dimensional Heisenberg antiferromagnet with a Néel temperature of 78 K, several of its intercalation compounds are found to exhibit spontaneous magnetization below around 40 K, giving the intercalation chemist a unique opportunity to influence the magnetic properties of a potentially processable layered system.[6,9,13-17]

A general understanding of the structural chemistry of the $MnPS_3$ intercalates may lead to some insights into the origins of the remarkable magnetic and optical properties of its molecular intercalation compounds. Therefore, we decided to attempt a detailed structural investigation of two prototypical systems, namely, $Mn_{1-x}PS_3\{G\}_{2x}(H_2O)_y$ for $G = Co(\eta\text{-}C_5H_5)_2^+$ [$x = 0.34$, $y = 0.3$] and $N(CH_3)_4^+$ [$x = 0.32$, $y = 0.9$]. Firstly, their relatively high degree of crystallinity makes them among the best candidates for structural studies of all the molecular intercalation compounds so far reported. Secondly, in the absence of a full structural investigation it has hitherto proved impossible to explain the dramatic differences in magnetic behavior between the pristine host lattice and its intercalation compounds.

The structural and physical properties of the MPS_3 lattices have been extensively studied and reviewed.[18] To a first approximation, these lattices can be thought of as adopting a $CdCl_2$ like structure in which the sulfur atoms adopt a cubic close packed array in which octahedral holes between adjacent layers are filled by either metal atoms ($^2/_3$ of the sites) or P−P pairs ($^1/_3$ of the sites). An alternative, and in light of its unusual intercalation chemistry, perhaps more informative picture of the structure is to view it not as a classical close-packed structure, but as an array of M^{2+} cations which are coordinated to $P_2S_6^{4-}$ bridging ligands so as to form two-dimensional slabs of formula $M_2P_2S_6$. This model is supported by the fact that the $P_2S_6^{4-}$ entity is well-known and characterized both in aqueous solution and in simple ionic compounds such as $Na_4P_2S_6$. Further support comes from the fact that these materials can be precipitated in an amorphous form by addition of the transition metal ion to a solution of $Na_4P_2S_6$ in methanol or acetonitrile.[10,14,19,20]

Single-crystal studies on a range of MPS_3 lattices (M = Mn, Fe, Co, Ni, Zn, Cd) have, however, shown that in most cases small distortions of the PS_3 groups away from trigonal symmetry lead to a monoclinic structure. Typical cell parameters (those of $MnPS_3$) are $a = 6.077$ Å, $b = 10.524$ Å, $c = 6.796$ Å, and $\beta = 107.35°$.[21,22] The relationship between this cell and a hexagonal cell is shown by the *b/a* ratio of 1.732 (i.e. $\sqrt{3}$) and depicted in Figure 1b. In fact, the Fe and Co phosphorous trisulfides can be satisfactorily refined on a hexagonal cell choice.

There are a number of pieces of evidence which suggest that $P_2S_6^{4-}$ is a highly flexible structural unit, and it is presumably this flexibility which gives rise to the unique ion exchange intercalation mechanism of these host lattices. Firstly, single-crystal studies have shown that while the P−S bond length remains essentially constant in these structures, the P−P distance varies as a function of metal radius, suggesting that these groups can "breath" and thus accommodate a range of cation sizes. The metal temperature factors, which could be correlated to crystal field stabilization energies, were also found to be fairly high, indicating that the metal ions are relatively weakly held in these lattices. The structural flexibility is further exemplified by compounds such as VPS_3 which has been shown to be non-stoichiometric: the actual formula being $V_{0.78}PS_3$ and best representation of the structure $V^{2+}_{0.34}V^{3+}_{0.44}PS_3$.[23,24] A range of mixed metal systems such as $M^IM^{III}P_2S_6$ (M^I = Ag, Cu; M^{III} = V, Cr) and $Mn_{0.87}Cu_{0.26}PS_3$ have also been reported where the lattice remains stable despite large distortions due to the presence of metal ions of markedly different radii in the former examples, and despite cation vacancies in the latter.[25-32]

(13) Clement, R.; Audiere, J. P.; Renard, J. P. *Rev. Chim. Miner.* **1982**, *19*, 560.
(14) Foot, P. J. S.; Nevett, B. A. *J. Chem. Soc., Chem. Commun.* **1987**, 380.
(15) Gledel, C.; Audiere, J. P.; Clement, R.; Cortes, R. *J. Mater. Sci.* **1988**, *7*, 1054.
(16) Gledel, C.; Audiere, J. P.; Clement, R.; Cortes, R. *J. Chim. Phys.* **1989**, *86*, 1691.
(17) Joy, P. A.; Vasudevan, S. *J. Am. Chem. Soc.* **1992**, *114*, 7792.
(18) Brec, R. *Solid State Ionics* **1986**, *22*, 3.
(19) Clement, R. P.; Davies, W. B.; Ford, K. A.; Green, M. L. H.; Jacobsen, A. J. *Inorg. Chem.* **1978**, *17*, 2754.
(20) Falius, H. *Z. Anorg. Allg. Chem.* **1968**, *359*, 189.
(21) Ouvrard, G.; Brec, R.; Rouxel, J. *Mater. Res. Bull.* **1985**, *20*, 1181.
(22) Prouzet, E.; Ouvrard, G.; Brec, R. *Mater. Res. Bull.* **1986**, *21*, 195.
(23) Ouvrard, G.; Freaur, R.; Brec, R.; Rouxel, J. *Mater. Res. Bull.* **1985**, *20*, 1053.
(24) Ouvrard, G.; Brec, R.; Rouxel, J. *C. R. Acad. Sci. Paris* **1982**, *294*, 971.
(25) Leblanc, A.; Rouxel, J. *C. R. Acad. Sci. Paris* **1980**, *291*, 263.
(26) Colombet, P.; Leblanc, A.; Danot, M.; Rouxel, J. *J. Solid State Chem.* **1982**, *41*, 174.
(27) Sourisseau, C.; Forgerit, J. P.; Mathey, Y. *J. Phys. Chem. Solids* **1983**, *44*, 119.
(28) Colombet, P.; Leblanc, A.; Danot, M.; Rouxel, J. *Nouv. J. Chim.* **1983**, *7*, 333.
(29) Lee, S.; Colombet, P.; Ouvrard, G.; Brec, R. *Mater. Res. Bull.* **1986**, *21*, 917.

Experimental Section

Synthesis of $MnPS_3$. A mixture of 1.810 g (32.95 mmol) of Mn (Koch, 99.98%), 1.021 g (32.95 mmol) of red phosphoros (Aldrich, 99.999%) and 3.200 g (99.81 mmol; 1% molar excess) of S (Aldrich, 99.999%) was intimately ground and sealed in a silica ampule under a vacuum of 10^{-4} Torr. The ampule was warmed slowly (1 °C/min) to 400 °C, left at this temperature overnight, and then warmed to 650 °C for 1 week. **Warning**, more rapid heating rates can cause the ampules to explode. Ampules were consequently wrapped in steel gauze and surrounded by a ceramic tube, then the tube furnace was placed behind safety screens. The resultant green powder was ground to <90 μm, then re-annealed with a 1% excess of S at 650 °C for an additional 7 days. Excess sulfur was removed by washing with CS_2. Sample purity was checked by X-ray diffraction.[3,18] Single crystals were synthesized by the vapor phase transport method using an iodine transport agent.[33-35] Approximately 2.0 g of the powdered material were sealed in a 25 cm × 1.5 cm i.d. silica ampule with 0.05 mg/cm^3 of the transport agent, and a linear 670−620 °C temperature gradient was applied along the ampule's length using a programmable 7-zone horizontal tube furnace. Heating times of 2 weeks resulted in full transport of the ampule contents, yielding *ca.* 2.0 g of transparent green plate-like crystals.

Guest Molecules. $Co(\eta\text{-}C_5H_5)_2$ was synthesized according to literature methods.[36] Perdeuteriocobaltocene, $Co(\eta\text{-}C_5D_5)_2$, was synthesized by the reaction of $Co(acac)_2$ with $Na(C_5D_5)$. Sodium metal (30.0 g) was added gradually to 250 cm^3 of deuterium oxide at 2 °C, yielding *ca.* 250 cm^3 of approximately 20% w/v NaOD in D_2O. A portion (50 cm^3) of this solution was added to 50 cm^3 of DMSO and 50 cm^3 of cyclopentadiene monomer. The mixture was stirred for 1 h, the cyclopentadiene monomer (top layer) decanted off, and the procedure repeated 4 times. The crude monomer was then distilled (40 °C) to give the pure deuterated monomer. Yield = 35.0 cm^3, 70%. The extent of deuteration was estimated to be >95% by mass spectroscopy. $Na(C_5D_5)$ was prepared by the dropwise addition of the deuterated monomer to finely divided sodium metal in THF, followed by 3 h of stirring at room temperature. The resulting mixture was filtered and the solvent removed under reduced pressure yielding a white powder.

$N(CD_3)_4Cl$ was prepared following a route suggested by Renaud.[37] A sample of 25 g of $N(CH_3)_4OH$ and 40 cm^3 of D_2O was placed in a stainless steel bomb and heated to 130 °C for 24 h. The contents of the bomb were then transferred to a schlenk and D_2O was removed into a liquid nitrogen cooled pre-trap under reduced pressure at 70 °C, yielding a white crystalline powder. This process was repeated 4 times, yielding 16.4 g of $N(CD_3)_4OD$. $N(CD_3)_4Cl$ was synthesized by reaction with a DCl/D_2O solution, and white crystals of $N(CD_3)_4Cl$ were obtained by recrystallization. Yield = 11.3 g, 31%. [Anal. Experimental: N, 10.43; C, 36.05; H, 10.1; Cl, 29.3. Expected: N, 10.48; C, 36.05; H, 9.89; Cl, 26.6 (based on $N(CH_3)_4Cl.0.6H_2O$).] The overall extent of deuteration was estimated by mass spectroscopy to be 94%.

Ion-exchange intercalation reactions of $MnPS_3$ were achieved by stirring a suspension of the powdered host in a 5 M aqueous solution of the guest species $[Co(Cp)_2^+I^-$ or $NMe_4Cl]$ at room temperature for *ca.* 24 h. Single crystals were intercalated in a similar manner, though the samples were not stirred to maintain the host crystallinity. Longer reaction times were employed to ensure complete intercalation. Direct insertion of cobaltocene was achieved by stirring a suspension of the host lattice in a toluene solution of cobaltocene at 120 °C for 3 days. Full intercalation was confirmed in each case by X-ray diffraction and elemental microanalysis. [Anal. Observed for $MnPS_3\{Co(Cp)_2\}_{0.39}$: C, 18.21; H, 1.60; Co, 8.9; Mn, 19.5. Calcd: C, 18.19; H, 1.53; Co, 8.9; Mn, 21.1. Observed for $Mn_{0.835}\{Co(Cp)_2\}_{0.33}(H_2O)_{0.3}$: C, 16.2; H, 1.4; Co, 7.7; Mn, 18.9. Calcd: C, 16.45; H, 1.62; Co, 8.1; Mn, 19.0. Observed for $Mn_{0.84}PS_3\{NMe_4\}_{0.32}(H_2O)_{0.9}$: C, 6.95; H, 2.45; N, 1.88. Calcd: C, 7.2; H, 2.64; N, 1.84.]

Techniques. X-ray diffraction patterns of both powdered samples and aligned single crystals were recorded in Bragg-Brentano (reflection) geometry on a Phillips PW1729 diffractometer, driven by a PW1710 controller and interfaced to an I.B.M.P.C. running Phillips APDv3.5 software. Cu Kα (α_1 = 1.54056 Å, α_2 = 1.54433 Å, weighted average = 1.54178 Å) radiation at 40 kV and 30 mA was used throughout. Samples recorded in transition mode were run as sealed capillaries or between sheets of Mylar on a Stöe Stadi-P diffractometer, with a 6 kW rotating anode Cu generator. Neutron diffraction patterns of $Mn_{1-x}PS_3\{G\}_x(D_2O)_y$ were recorded for G = $Co(\eta\text{-}C_5D_5)_2$ and $N(CD_3)_4$ with a wavelength of 2.426 Å using the "Pyrrhias" powder diffractometer (G4.1) at the Orphée reactor source at the Léon Brillouin Laboratory, Saclay, France. Low temperature was achieved using an "ILL Orange Cryostat". Further details of the experimental setup are given in the Users' Guide published by the Léon Brillouin Laboratory.[38]

Single crystals of the intercalation compounds were selected by optical microscopy, and their crystallinity was checked by oscillation and Weissenberg photography. Photographs were recorded on a Stöe Weissenberg camera using an Enraf-Nonius Cu Kα X-ray source and Agfa-Gevaert Osray M3 X-ray film. Crystals were aligned along their *a* axis by a series of oscillation photographs, using exposure times of up to 12 h for weakly diffracting crystals. Weissenberg photographs were recorded using a 3 mm slit width and exposure times of between 1 and 7 days.[39]

Automated diffractometer studies were performed using an Enraf-Nonius CAD-4 diffractometer. Crystals were initially visually centered on the CAD-4, then aligned with their *a* axis parallel to the goniometer axis by oscillation photography. Weissenberg photographs were also recorded to check the crystallinity of the sample and identify strong reflections. The goniometer was then transferred directly to the CAD-4 and the 00*l* reflections found and centred using an $\omega-2\theta$ scan mode. Attempts to center these broad reflections in ω proved unsuccessful. Several strong non-00*l* reflections were located and centered from rotation photographs, and these were indexed on the basis of the information from powder diffraction patterns and the Weissenberg photographs. The positions of two strong reflections and approximate unit cell parameters from powder studies were then used to determine an orientation matrix from which 24 strong reflections were located and centered. Reflections were indexed on the basis of cell parameters closely related to those of the pristine host, and the cell was refined. Cell parameters were the following: $Mn_{0.83}PS_3\{Co(Cp)_2\}_{0.34}(H_2O)_{0.3}$, a = 6.108(3) Å, b = 10.562(4) Å, c = 11.833(5) Å, α = 90.05(3)°, β = 85.18(4)°, γ = 90.06(3)°; $Mn_{0.84}PS_3\{NMe_4\}_{0.32}(H_2O)_{0.9}$, a = 18.31(3) Å, b = 10.59(1) Å, c = 11.53(1) Å, α = 90.2(1)°, β = 90.0(1)°, γ = 90.0(1)°.

Solid state ^2H NMR spectra were recorded at 30.7 and 61.4 MHz using a Bruker MSL 200 or a Bruker MSL 400 spectrometer with a high-power probe containing a horizontal solenoid insert. Air-sensitive samples were sealed in 5 mm diameter Pyrex tubes using a plug of epoxy resin. Single crystals were again mounted within Pyrex tubes and visually aligned with their *c* axis either parallel or perpendicular to the spectrometer field. Spectra were recorded using the quadrupole echo sequence with spin−echo delays in the range 20−50 μs and recycle delays in the region 0.2−10 s.[40-42] Details of spectral acquisition parameters are given in the relevant figure captions. Further details of the spectrometer setup and data collection methods are given elsewhere.[43]

^{31}P CP/MAS NMR spectra were recorded at 81.02 MHz using a Bruker MSL 200 spectrometer equipped with a multinuclear proton

(30) Burr, G.; Durand, E.; Evain, M.; Brec, R. *J. Solid State Chem.* **1993**, *103*, 514.
(31) Mathey, Y.; Michalowicz, A.; Taffoli, P.; Vlaic, G. *Inorg. Chem.* **1984**, *23*, 897.
(32) Lee, S.; Colombet, P.; Brec, R. *Inorg. Chem.* **1988**, *27*, 917.
(33) Nitsche, R.; Bölsterli, H. U.; Lichtensteiger, M. *J. Phys. Chem. Solids* **1961**, *21*, 199.
(34) Nitsche, R.; Wild, P. *Mater. Res. Bull.* **1970**, *5*, 419.
(35) Balchin, A. A. In *Crystallography and Crystal Chemistry of Materials with Layered Structures*; Levy, F., Ed.; D. Riedel: Dordrecht, 1976; Vol. 1, p 1.
(36) Wilkinson, G.; Cotton, F. A.; Birmingham, J. M. *J. Inorg. Nucl. Chem.* **1956**, *2*, 95.
(37) Renaud, R. N.; Leitch, L. C. *Can. J. Chem.* **1968**, *46*, 385.
(38) *Equipements Experimentaux*; Laboratiore Léon Brillouin: Saclay, France, 1987.
(39) Henry, N. F. M.; Lipson, H.; Wooster, W. A. *The Interpretation of X-ray Diffraction Photographs*, 2nd ed.; Macmillan: New York, 1961.
(40) Davis, J. H.; Jeffrey, K. R.; Bloom, M.; Valic, M. I.; Higgs, T. P. *Chem. Phys. Lett.* **1976**, *42*, 390.
(41) Bloom, M.; Davis, J. H.; Valic, M. I. *Can. J. Phys.* **1980**, *58*, 1510.
(42) Hentschel, R.; Spiess, H. W. *J. Magn. Reson.* **1979**, *35*, 157.
(43) Mason, S. D. Phil. Thesis, Oxford, 1993.

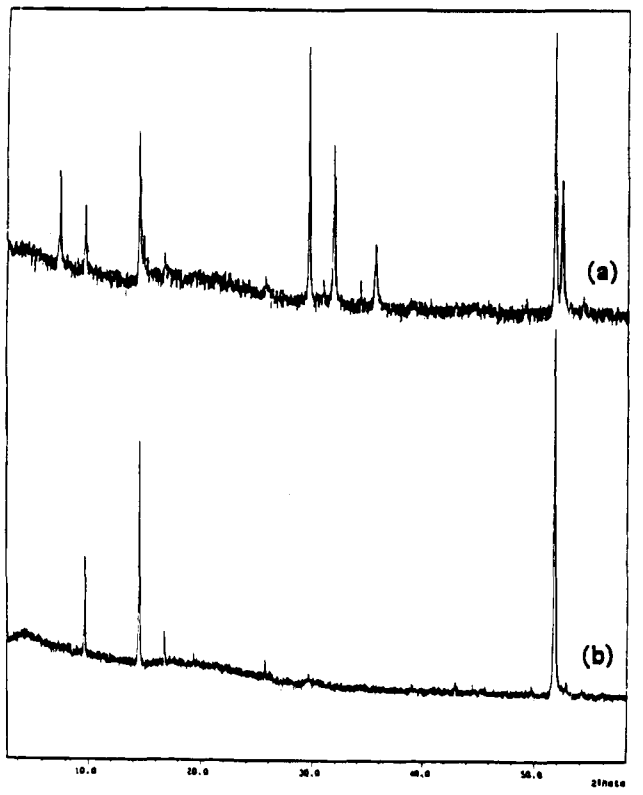

Figure 2. (a) Powder X-ray diffraction pattern of $Mn_{0.83}PS_3\{Co(Cp)_2\}_{0.34}(H_2O)_{0.3}$. (b) X-ray diffraction pattern of an aligned single crystal run in transmission mode to record *hk*0 reflections only. All "superlattice" reflections in (a) are also present in (b).

enhanced, double-bearing magic-angle sample spinning probe (Bruker Z32-DR-MAS-7DB) and a high-power proton decoupler. Samples were spun at speeds of 2−3 kHz. Pulse lengths of 90° in the range 6−8 μs and recycle delays of 1.0 s were employed.

Results and Discussion

The results of the structural studies on the ion-exchange intercalates of $MnPS_3$ will be presented in three main sections for clarity. Firstly the results for the $Co(Cp)_2$ intercalates will be presented, then those on the tetramethylammonium intercalate. Finally, the results from the two sections will be collated to give an overall view of the structures of these intercalates.

1. Cobaltocene Intercalates of $MnPS_3$. (a) Powder Diffraction Studies. The powder X-ray diffraction pattern of the ion-exchange synthesized sample, $Mn_{0.83}PS_3\{Co(Cp)_2\}_{0.34}(H_2O)_{0.3}$, obtained from a capillary-mounted sample on a Stöe powder diffractometer is shown in Figure 2a. From this spectrum it is clear that the material is highly crystalline and exhibits a number of sharp diffraction peaks. Previous studies on this material reported that the powder pattern could be indexed on a unit cell closely related to that of the pristine host lattice, but with an expanded *c* axis, caused by the intercalation of the guest molecule. The reported cell dimensions were a = 6.117 Å, b = 10.59 Å, c = 12.53 Å, β = 109° (pristine $MnPS_3$ has a = 6.077 Å, b = 10.524 Å, c = 6.796 Å, β = 107.35°), showing that an increase in the interlamellar separation of *ca.* 5.46 Å occurs on intercalation. This is similar to the expansions found for other layered sulfide lattices.[44,45] While the majority of the peaks observed in these two studies correspond, a number of the strongest peaks of Figure 2 were not previously reported, and in particular the peak observed at 2θ = 9.627° (d = 9.179 Å) could not be indexed using the published cell parameters (see Table 1).

Table 1. Peaks Visible in the Powder Diffraction Pattern of an Aligned Single Crystal of $Mn_{0.83}PS_3\{Co(Cp)_2\}_{0.34}(H_2O)_{0.3}$, and Their Indices Based on the Various Unit Cell Choices discussed in the Text (a = 6.12 Å, b = 10.60 Å)

$2\theta_{obs}$	d_{obs}/Å	intensity	cell I[a] *a b*	cell II 3*a b*	cell III $2\sqrt{3}a$ (γ = 120°)	cell IV 6*a b*
9.613	9.193	27.4	*	2 0 0, 1 1 0	2 0 0	4 0 0
14.464	6.119	60.7	1 0 0	3 0 0	3 0 0	6 0 0
16.672	5.313	29.1	0 2 0	0 2 0, 3 1 0	2 2 0	0 2 0
19.311	4.593	4.4	*	4 0 0, 2 2 0	4 0 0	8 0 0
38.993	2.308	18.6	2 3 0	8 0 0, 4 4 0	6 3 0	16 0 0
49.691	1.833	3.7	*	10 0 0, 5 5 0	10 0 0	20 0 0
51.704	1.767	94.7	0 6 0	0 6 0, 9 3 0	6 6 0	0 6 0
60.754	1.523	8.2	4 0 0	12 0 0, 6 6 0	12 0 0	24 0 0
83.829	1.153	5.2	4 6 0	16 0 0, 8 8 0	16 0 0	32 0 0
98.609	1.016	4.7	6 0 0	18 0 0, 9 9 0	18 0 0	36 0 0

[a] An asterisk represents peaks that cannot be indexed on the given cell.

Since large single crystals of this compound which have an easily identifiable *c* axis were available, the diffraction pattern of an aligned single crystal was recorded in both reflection geometry (where only 00*l* reflections are recorded) and transmission geometry (where only *hk*0 reflections are observed). In this manner it is possible to separate the 00*l* and *hk*0 reflections from the more general *hkl* reflections of the powder diffraction pattern, which greatly increases the ease with which the pattern may be indexed. The *hk*0 spectrum is shown in Figure 2b. Since there have been some reports in the literature that the physical properties of single-crystal and powdered samples of certain intercalation compounds can show subtle differences, the powder X-ray profile of a crushed sample of crystals was initially recorded.[45] This confirmed that samples synthesized using both powdered and single-crystal starting forms of the host lattice exhibit identical diffraction patterns.

It can be seen from Figure 2 that all the diffraction peaks in the powder (*hkl*) pattern of Figure 2a which could not be indexed on the published cell are also present in the *hk*0 diffraction pattern. This suggests that the true unit cell required to fully index the powder pattern, while being related to that previously reported, is considerably larger in the *ab* plane. The observed pattern could be fully indexed on a cell with an *a* axis three times that of the pristine host. The major *hk*0 peaks observed and their indices on this tripled cell (denoted cell choice II for clarity) are given in Table 1. In the light of the single-crystal studies (*vide infra*) it is, however, more enlightening to ignore the small distortions of the pristine lattice which lead to the adoption of a monoclinic cell, which will be grossly affected by intercalation, and adopt a hexagonal unit cell to reflect the local symmetry of the host layers. Thus the data can be more conveniently indexed on a hexagonal cell with $a' = b'$ = 21.22 Å (i.e. 2 × $2\sqrt{3}a$ of the original lattice). This is shown as cell choice III in Table 1. The various cell choices and their relationship to the pristine lattice are shown in Figure 3.

Further evidence for the formation of a superlattice in the *ab* plane of this intercalate was obtained by powder neutron diffraction experiments on a fully deuterated sample of the intercalate which will be reported in more detail elsewhere.[46] The most noteworthy features of the room temperature spectrum were the observation of a weak diffraction peak at d = 9.1 Å, again indicating the existence of a superlattice in the *ab* plane, and a broad diffraction peak corresponding to a *d*-spacing of *ca.* 5.2 Å (i.e. around the position expected for the 020 reflection

(44) Michalowicz, A.; Clement, R. *Inorg. Chem.* **1982**, *21*, 3872.
(45) O'Hare, D.; Evans, J. S. O. *Comments Inorg. Chem.* **1993**, *14*, 155.
(46) Evans, J. S. O.; O'Hare, D.; Clement, R. Manuscript in preparation.

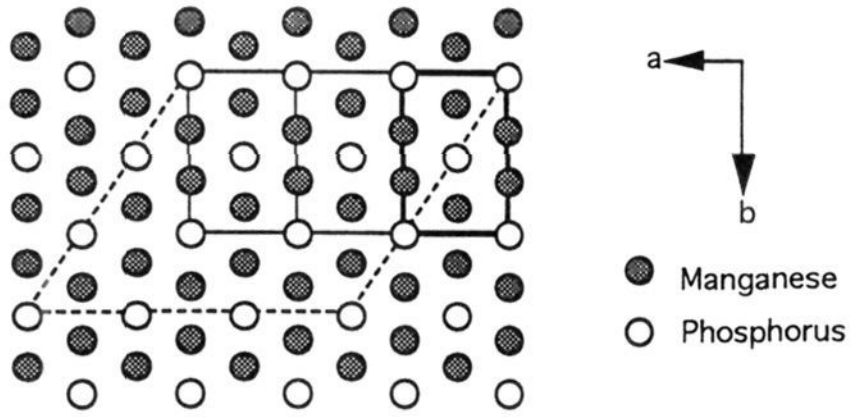

Figure 3. The three cell choices used to index the *hk*0 spectrum of $Mn_{0.83}PS_3\{Co(Cp)_2\}_{0.34}(H_2O)_{0.3}$. A bold solid line represents cell choice I (6.1 × 10.6 Å); a light solid line represents cell choice II (18.3 × 10.6 Å), and a dashed line represents cell choice III (21.2 × 21.2 Å, $\gamma = 120°$).

of cell choices I and II). The line shape of this peak was strongly reminiscent of that obtained by Warren for turbostatic graphite, suggesting the presence of significant 2D disorder in the neutron scattering of this material.[47] Lattice imaging experiments were also attempted using a Jeol 2000FX electron microscope, but it only proved possible to observe lattice fringes corresponding to plane separations expected from cell choice I; no further evidence for the proposed superlattice was obtained.

The ^{31}P NMR spectra of pristine $MnPS_3$ and a variety of its intercalates were also recorded in the hope that information about metal vacancy sites could be obtained. These revealed, however, that the phosphorus environment becomes sufficiently disordered on intercalation that all peaks are broadened into the baseline, and little information could be extracted by this technique.

There is then considerable evidence from the powder diffraction data for the existence of a superlattice in the *ab* plane of this compound. Two possible sources for this can be proposed; firstly, it could be caused by an ordering of the metal vacancy sites which are formed during intercalation within the host lattice layers. Secondly, the packing of the guest molecules could give rise to such features, as previously proposed for many graphite intercalation compounds. These two possibilities are discussed in more detail below.

(b) Single-Crystal Studies on $Mn_{0.83}PS_3\{Co(Cp)_2\}_{0.34}(H_2O)_{0.3}$. Despite the inherent disorder and poor crystallinity of crystals of these layered intercalates, attempts were made at single-crystal structure determination using standard automated diffractometry techniques. Due to the extreme broadness of the reflections, automatic peak search routines proved impossible. Instead two reflections were located from Polaroid photographs and centred by $\omega-2\theta$ scans. These reflections were indexed on the basis of cell choice I of Table 1 (i.e. on a cell closely related to that of the pristine host lattice) and used to find an additional 22 reflections. From these reflections the unit cell was refined, giving the final cell parameters a = 6.108(3) Å, b = 10.562(4) Å, c = 11.835(5) Å, and β = 85.18(4)°.

Data collection on this cell gave a total of just 202 reflections which passed the $I > 3\sigma$ cutoff, again due to the extreme broadness of the diffraction peaks. Examination of peak intensities revealed that all strong reflections belonged to the class $k = 3n$, suggesting a unit cell with a b axis one-third that used for data collection (i.e. on a cell of a = 6.11 Å, b = 3.52 Å, c = 11.833 Å, β = 85.18°), and suggesting the possibility of disorder in the crystal; this disorder will be discussed in more detail below. Structure solution was attempted by Patterson synthesis, followed by introduction of manganese and sulfur atoms, and subsequent least-squares refinement. It proved impossible, however, to achieve a chemically sensible structural model which accurately modeled the observed intensity data.

(47) Warren, B. E. *Phys. Rev.* **1941**, *59*, 693.

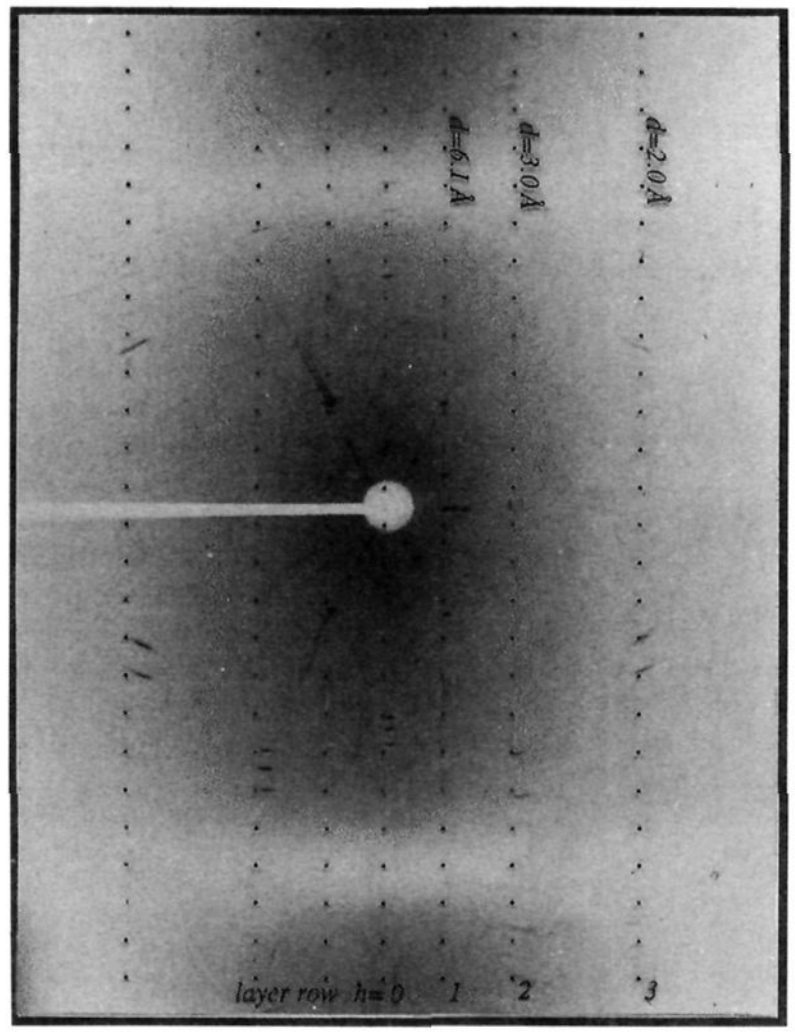

Figure 4. Single-crystal oscillation photograph of $Mn_{0.83}PS_3\{Co(Cp)_2\}_{0.34}(H_2O)_{0.3}$ mounted along its a axis. In addition to strong reflections corresponding to h = 1, 2, 3, weak additional reflections are also visible suggesting an increase in cell dimensions.

To further investigate this structure, a series of oscillation and Weissenberg photographs of the same crystal were taken. Figure 4 shows a 2 h exposure oscillation photograph taken with the crystal mounted along its a axis. From this photograph it can be seen that in addition to strong reflections corresponding to h = 1, 2, 3, and 4 reciprocal lattice rows, a further series of inner reflections are observed which can only be indexed on the basis of a considerably enlarged cell. Observed layer separations and their relationship to cell choice I (that with a and b dimensions essentially identical to the pristine host) are shown in Table 2. It can be seen that these data are in accordance with the conclusions of the powder diffraction data, and in fact suggest that the intercalation compound has a unit cell some six times as large as the pristine host in the a direction.

Weissenberg photographs of the h = 0 and 2 (based on cell choice I) layers are shown in Figure 5, parts a and b. The principal features of the 0*kl* photograph (Figure 5a) are then the sharp series of spots lying across the main diagonal of the photograph, which correspond to the 00*l* reflections, and the "festoons" of spots which correspond to the 06*l* and 0 12 *l* reflections. As such the photograph appears to contain far fewer reflections than would be expected if the intercalated lattice could still be accurately described in terms of a unit cell analogous to that of the host material. In particular, no reflections of the category 02*l* or 04*l* are observed, many of which are strong reflections for $MnPS_3$, and are observed for the pristine host. Careful examination of the films, however, reveals the presence of lines of diffuse scatter along the reciprocal lattice rows where one would expect to see these classes of reflections (Figure 5a).

This again indicates that there is now considerable disorder present in the lattice, and that while the diffraction could be

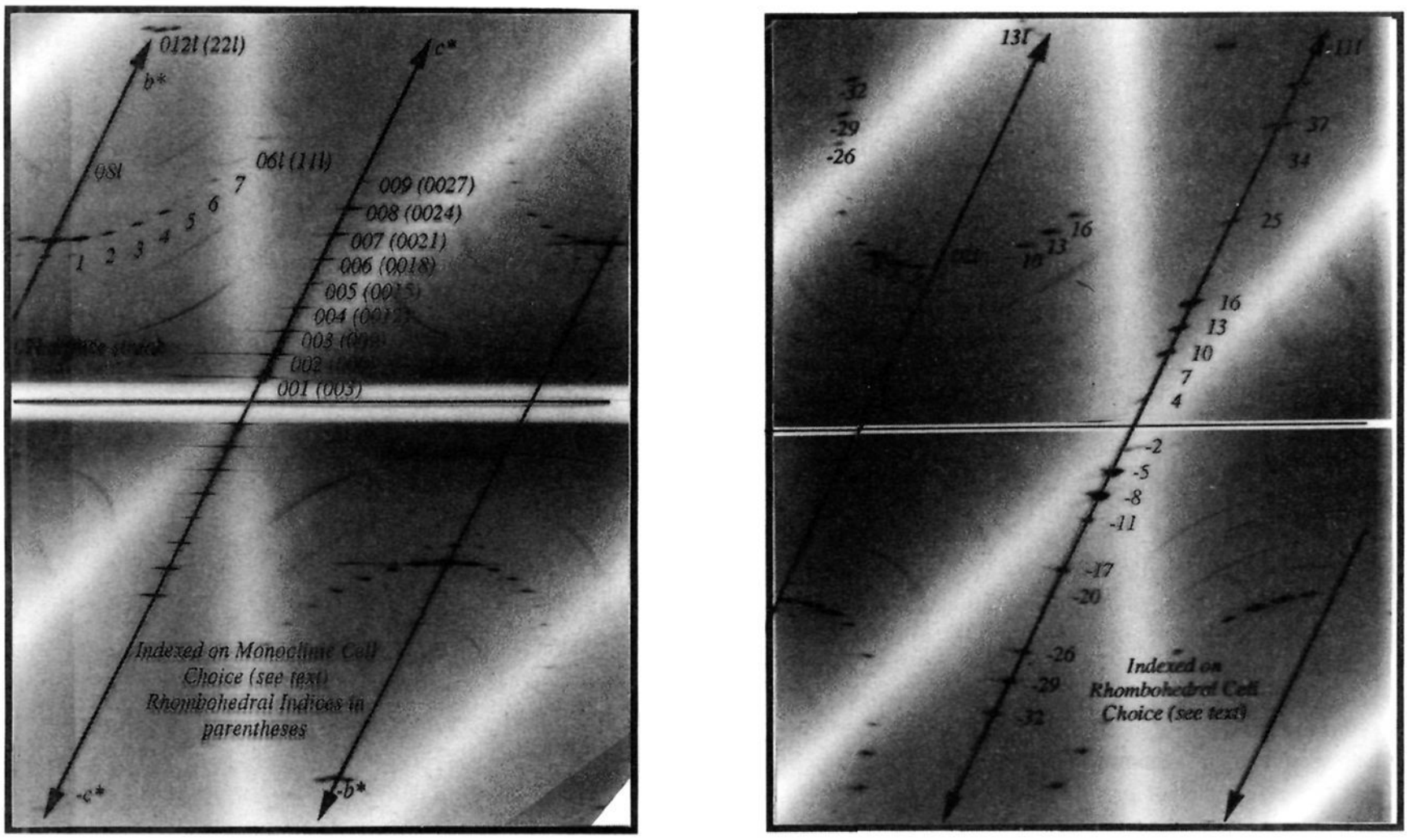

Figure 5. (a, left) Weissenberg photograph of the $h = 0$ layer of $Mn_{0.83}PS_3\{Co(Cp)_2\}_{0.34}(H_2O)_{0.3}$ taken using an exposure time of 7 days and of the (b, right) $h = 2$ layer with a 4 day exposure.

Table 2. Unit Cell Parameters from the Oscillation Photograph of Figure 4[a]

separation of layer lines/mm	d/Å	relationship to cell I
4.8(1)	18.4(4)	3*a*
7.2(1)	12.3(2)	2*a*
9.7(1)	9.1(1)	1.5*a*
14.9(1)	6.12(3)	a
33.5(5)	3.05(3)	*a*/2
66.0(10)	2.04(1)	*a*/3

[a] The numbers in parentheses show the estimated errors in the measurements. d spacings were calculated using the relationship $d^* = 1/\lambda \sin[\tan^{-1}(h/r)]$ where h is the spot height and r is the camera radius.

described in terms of a monoclinic cell with a and b dimensions essentially identical to those of $MnPS_3$, all the observed peaks could equally be described in terms of a considerably smaller lattice. Thus all the diffraction peaks in the zero layer photograph can be described in terms of a cell with a b axis one-third that of $MnPS_3$ (i.e. on a cell 6.1 × 3.52 × 11.83 Å).

A potential source of this disorder can be seen if one considers the effect that intercalation is likely to have on Mn/P site ordering between adjacent layers. In pristine $MnPS_3$ the layer stacking sequence is such that the same lattice sites are occupied by either metal atoms or phosphorus pairs in each lattice layer. This gives an ordered Mn/P array in three dimensions. The process of intercalation, however, forces the host lattice layers to increase their separation by over 5 Å. Even if the sulfur atoms subsequently lock into definite lattice positions, giving an ordered sulfur array, unless the guest layer is itself highly ordered it is extremely unlikely that any registry between adjacent layers is retained. Even though individual layers of the intercalation compound contain an ordered array of metal atoms and phosphorus pairs, the crystal as a whole will contain disordered manganese/phosphorus sites. Such a disordering process is shown schematically in Figure 6.

The unit cell required to describe the diffraction from the overall crystal is then considerably smaller than that needed to describe the order within an individual ab plane, and a number of cell choices are again possible. One obvious cell choice to choose from the above description is simply based upon $a \times b/3 \times c$ of the pristine host. A second possible cell choice which appears to describe the reflections of the zero layer Weissenberg well is a hexagonal cell with dimensions $b/3$ of the original cell. There are two reasons for adopting this cell. Firstly such a cell choice reflects the local symmetry of an individual layer, and secondly it allows a direct comparison to be made between $MnPS_3$ and the better understood metal dichalcogenide systems. This cell choice, and its relationship to the original lattice, is shown in Figures 6 and 7.

The reflections observed on the zero level Weissenberg can then be reindexed on such a cell choice. From Figure 7 it can be seen that the crystal can now be considered as being mounted along its [110] axis. Thus on the new cell choice what were the 06l reflections can be reindexed as the 11l reflections, and what were the 0 12 l become the 22l reflections.

Examination of the second layer Weissenberg (Figure 5b) reveals, however, that the actual unit cell is more complicated than that suggested by the zero layer. Based upon a hexagonal cell choice, the observed reflections correspond to the $2\bar{2}l$ reflections (main diagonal) and the 40l and 62l reflections (festoons of spots). The observed spots cannot, however, be indexed on the simple hexagonal cell of Figure 7, but suggest a unit cell which has a tripled c axis. On this basis the observed reflections can be successfully indexed as the $\bar{1}1l$ series ($l = -32, -29, ..., 1, 4, 7, ..., 34, 37$), the 02$l$ series ($l = -32, -29, ..., 34, 37$), and the 13$l$ series ($l = -8, -5, -2$). On such a tripled unit cell, the zero layer Weissenberg must be reindexed as containing the 00l ($l = 3n$) and hhl ($l = 3n$) reflections.

This tripling of the hexagonal c axis, together with the intensity distribution observed, then suggests a rhombohedral space group with reflection conditions $-h + k + l = 3n$. For the specific categories of reflections present on the films

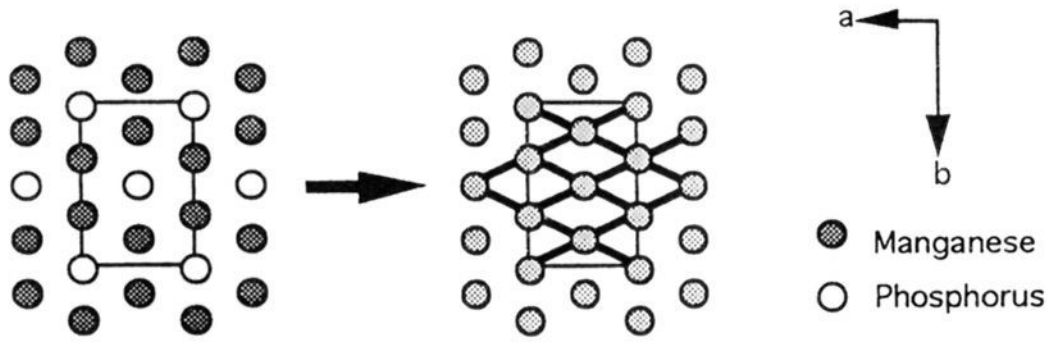

Figure 6. Schematic representation of how total Mn/P disordering leads to a reduction in cell dimensions from a rectangular $a \times b$ cell to a hexagonal $b/3 \times b/3$, $\gamma = 120°$ cell. The hexagonal cell is shown by bold solid lines.

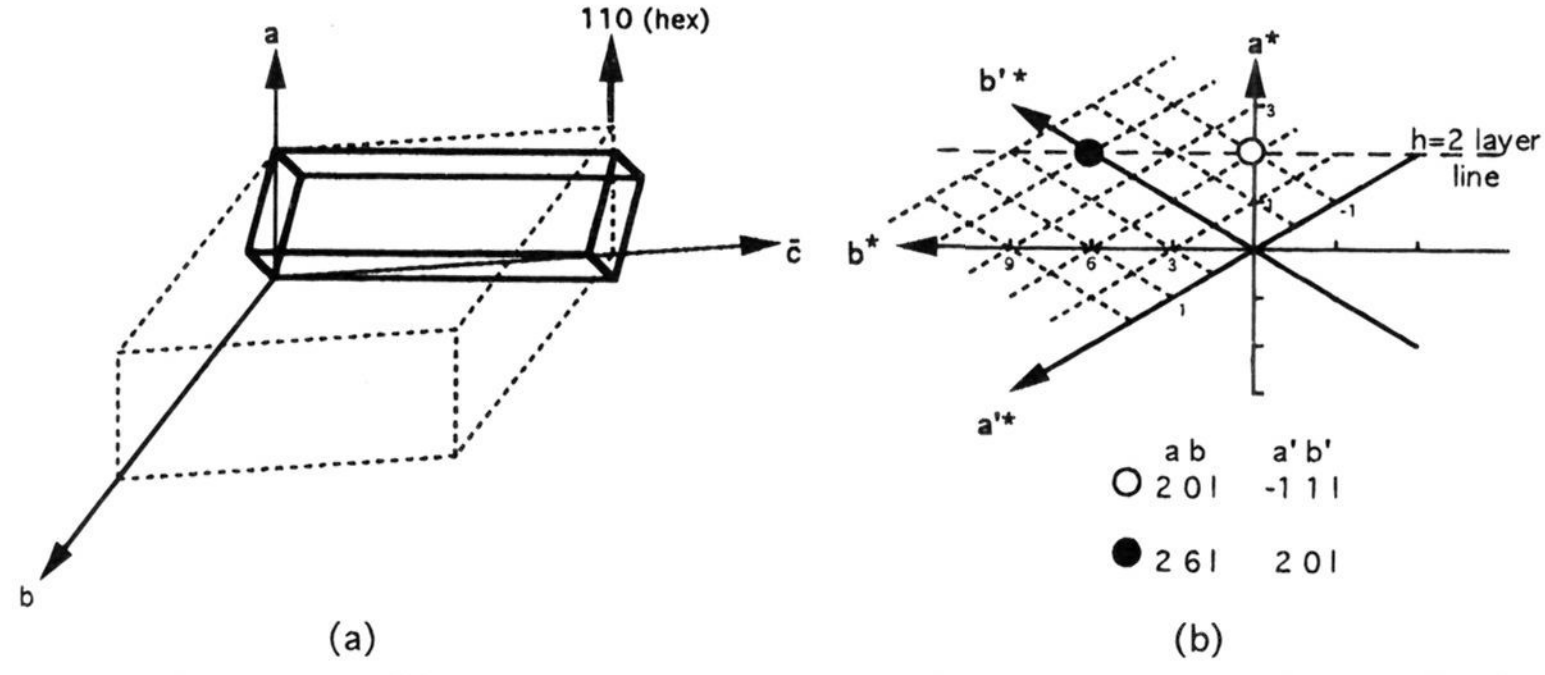

Figure 7. Relationship between a monoclinic cell choice and the proposed hexagonal cell. (a) Three-dimensional representation of the two cells, with the hexagonal cell shown in bold. (b) The relationship between the reciprocal cell axes of the original (a^*, b^*) and hexagonal (a'^*, b'^*) cells showing how the "zero" layer photograph (Figure 5a) contains the $h\ h\ l$ layer and the 2nd layer (Figure 5b) the $h\ h{+}4\ l$ reflections of the new cell.

recorded this condition implies that reflections will only be observed on the "zero" layer for $00l$ and hhl ($l = 3n$) and on the "second" layer for $\bar{1}1l$, $02l$, and $13l$ ($l = 3n + 1$).

This change in symmetry of the host lattice can then be rationalized in terms of the same intercalation induced shifts of host lattice layers in the *ab* plane which were invoked above to explain the introduction of Mn/P site disordering. Given the observation of relatively sharp hkl ($l \neq 0$) reflections in the photographs of Figure 5, the intercalation compound must have a reasonable degree of three-dimensional order. This shows that registry is retained between sulfur atoms of subsequent layers and therefore suggests the presence of specific interactions between the guest molecules and host layers. Since this in turn implies that the guest molecules adopt certain low-energy sites between the layers, it is reasonable to assume that the relative displacement of adjacent layers is driven by the adoption of a symmetrical sulfur environment by the intercalated cobaltocenium molecules such that a trigonal prismatic sulfur environment is achieved. There are two possible ways in which such an arrangement could occur, as shown in Figure 8. Firstly a rotation of alternate layers by 60° relative to their position in the pristine host would require a doubling of the c axis and lead to a lattice of overall symmetry $P\bar{6}3/mmc$; secondly, a translation of adjacent layers by $(+a/6, +b/2)$ on the monoclinic cell choice (cell I), which corresponds to a shift of $(1/3)^{1/2}a$ along the hexagonal [110] axis of Figure 7, would require a tripling of the c axis and lead to a lattice of overall symmetry $R\bar{3}m$.

Clearly the second alternative appears to fit the information of the Weissenberg photographs extremely well, and calculations reveal a good general agreement between observed intensities and those calculated for such a structure. A model is therefore proposed for this layer shift whereby cobaltocene molecules adopt specific interlamellar sites and attain a sulfur coordination environment which is symmetrical above and below the layer of guest molecules. It is then these specific guest−host interactions which give rise to the high degree of crystallinity in these compounds.

Such a model also explains both the unit cell obtained by the CAD-4 studies and the subsequent failure of structural refinement. The relationship between the CAD-4 cell and the true tripled rhombohedral cell is shown in Figure 8c. It can be seen that the experimentally refined β angle of 85.14°, for a c axis of 11.83 Å, corresponds to an "offset" between adjacent layers of some 1.0 Å (i.e. $11.83 \times \cos\{90-85.14\}$). Given the observed cell dimension of $a = 6.11$ Å, this corresponds to a shift of precisely **a**/6 between subsequent layers. This is exactly the shift proposed to explain the symmetry changes of the Weissenberg photographs. The incorrect cell choice and resultant incomplete data set recorded explains the failure of the CAD-4 data to give satisfactory structural refinement. The non $hk0$ reflections of the powder pattern of Figure 2 can also be fully indexed on such a cell choice; the refined cell parameters are $a = b = 3.532(2)$ Å, $c = 35.57(2)$ Å, $\alpha = \beta = 90°$, and $\gamma = 120°$.

Powder X-ray and neutron diffraction patterns were also recorded on the cobaltocene intercalate of $MnPS_3$ synthesized by direct reduction, $MnPS_3\{Co(Cp)_2\}_{0.39}$. These were essentially similar to those of the compound prepared by ion-exchange intercalation, though in this case no reflections corresponding to a possible superlattice were observed. In particular, no evidence for the 9.1 Å peak, which featured so prominently in the previous compound, was observed. Single-crystal oscillation and Weissenberg photographs of this compound were also recorded. Oscillation photographs again

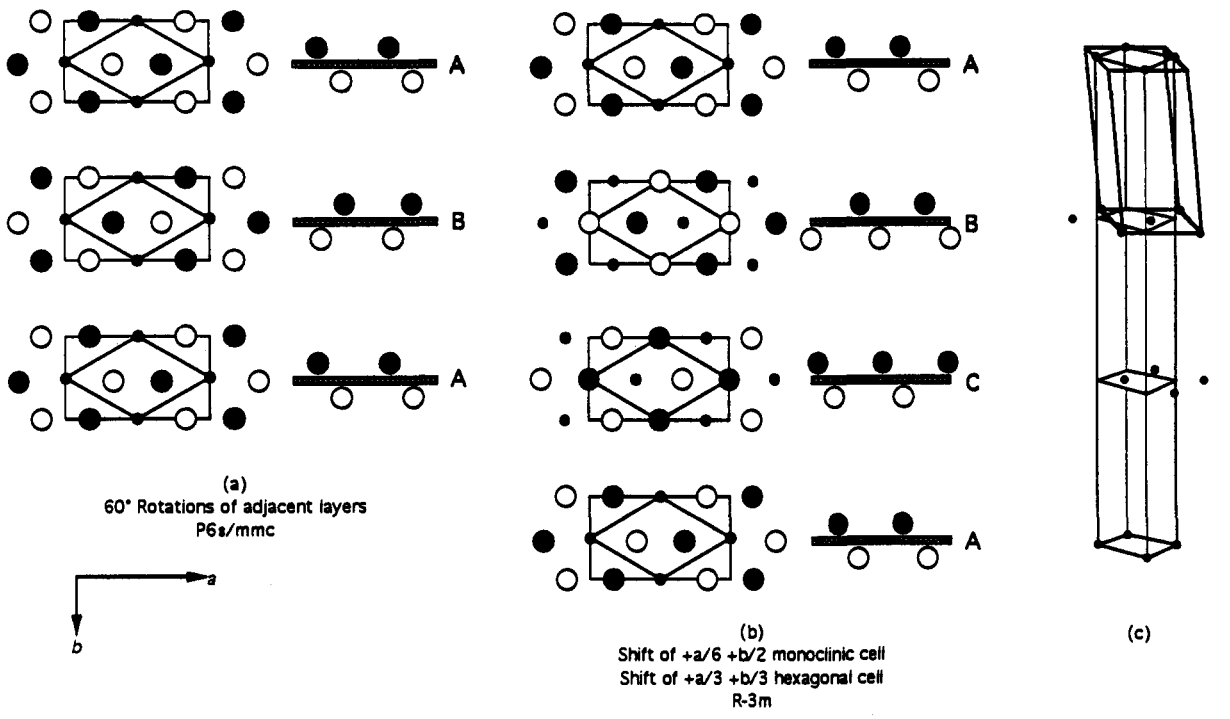

Figure 8. Layer shifts in $MnPS_3\{Co(Cp)_2\}_{0.34}(H_2O)_{0.3}$. Schematic representation of *the ab* plane of the cell, and side view emphasizing the alignment of S atoms: (●) S above a layer and (○) S below a layer. (a) Rotation of adjacent layers by 60° gives rise to a two-layer repeat structure (ABABA...), symmetry *P*6*3*/*mmc*; (b) translation of adjacent layers gives a three-layer repeat structure (ABCABCA...), space group $R\bar{3}m$. (c) Relationship between the rhombohedral cell of (b) and the monoclinic cell found by the CAD-4; monoclinic cell shown in bold lines.

showed no evidence for any superlattice reflections in these compounds. Zero level Weissenberg photographs were very similar to those of Figure 5 in that no order beyond the 06*l* level was discernible, again indicating the existence of Mn/P disorder between subsequent layers of the lattice and the possibility of adopting a reduced unit cell. The lower degree of crystallinity of these compounds, as evidenced by the somewhat broader nature of the reflections observed in ω, precluded further work.

(c) ^{2}H Solid-State NMR Studies. The diffraction techniques already discussed provide much information about the structure of the host lattice layers and the changes which they undergo on intercalation. Diffraction techniques are not, however, well-suited to the study of the guest molecules, which are frequently disordered in these compounds, and have many motional degrees of freedom. For these reasons it was decided to use ^{2}H solid-state NMR to probe the orientational preferences of the guest molecule and to investigate their motional behavior.

The principal interactions between the quadrupolar ($I = 1$) ^{2}H nucleus and an applied magnetic field are the Zeeman and quadrupolar terms. For a single crystal which presents a single deuterium orientation to the applied field, a doublet is observed in the ^{2}H NMR spectrum, with the magnitude of the doublet separation reflecting the angle of the principal component of the electric field gradient tensor at the deuterium nucleus to the applied field. For a polycrystalline sample, the random distribution of crystallites presents all orientations of the C−D bond to the field and the resulting spectrum represents the superposition of a range of doublets, giving a characteristic "Pake Doublet" line shape. Since both the doublet separation and hence the line shape of the powder spectrum are extremely sensitive to motions of the C−D bond (and in particular to motions in the range 10^3-10^8 Hz), solid-state deuterium NMR is an extremely powerful tool for investigating the orientation and dynamics of intercalated guest molecules and has been successfully applied in several such studies.[43,48-52]

Two low-energy orientations have been postulated for metallocene molecules between the layers of lamellar host lattices, with the principal C_5 molecular axis either parallel or perpendicular to the host layer planes (see Figure 9).[45] These two orientations can be probed by performing ^{2}H NMR experiments on an aligned single crystal of the sample.

Since the cyclopentadienyl rings in these compounds undergo rapid rotation around the C_5 molecular axis, the electric field gradients of the individual deuterium nuclei become averaged such that the overall effective tensor is oriented along the principal axis of the molecule, and thus serves as a direct indicator of the guest orientation. By aligning a single crystal with its *c* axis parallel to the spectrometer field, it then becomes possible to distinguish the two orientations of the guest molecules. A guest oriented with its principal molecular axis perpendicular to the layers would be expected to give rise to a doublet separation of $^3/_4$ of the nuclear quadrupole coupling constant, or for the case of an aromatic C−D bond approximately 140 kHz, whereas in the case of the parallel orientation this would be reduced to *ca.* 70 kHz.

Further information can be obtained about the in-plane motion of the guest molecules by orienting the crystal such that the applied field is parallel to the host layers. For the parallel guest orientation if the molecules rotate about their C_2 molecular axis at a rate which is fast on the NMR time scale ($>10^8$ Hz) then a further reduction in the doublet separation to *ca.* 33 kHz results. If, however, the molecules are static, with a random orientation of their molecular axis in the *ab* plane, then a powder line shape would be expected.[43] These various spectral possibilities are summarized in Figure 9 for clarity.

(48) Lifshitz, E.; Vega, S.; Luz, Z.; Francis, A. H.; Zimmerman, H. *J. Phys. Chem. Solids* **1986**, *47*, 1045.
(49) McDaniel, P. L.; G. Liu; Janas, J. *J. Phys. Chem.* **1988**, *92*, 5055.
(50) Heyes, S. J.; Clayden, N. J.; Dobson, C. M.; Green, M. L. H.; Wiseman, P. J. *J. Chem. Soc., Chem. Commun.* **1987**, 1560.
(51) Heyes, S. J. D. Phil Thesis, Oxford, 1989.
(52) Grey, C. P.; Evans, J. S. O.; O'Hare, D.; Heyes, S. J. *J. Chem. Soc., Chem. Commun.* **1991**, 1381.

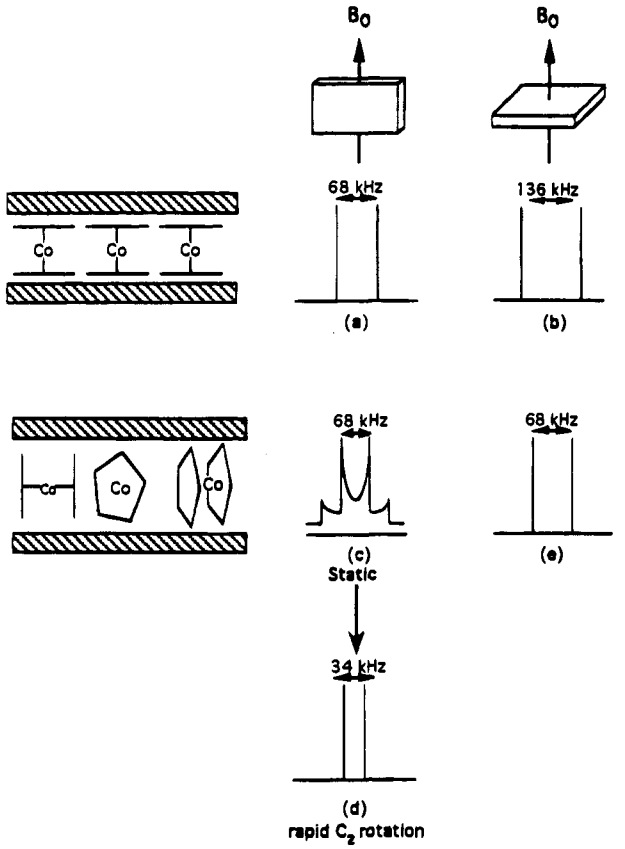

Figure 9. Simulations of the single-crystal ^2H NMR spectra expected for aligned single crystals of a metallocene intercalation compound. If the molecules adopt the perpendicular orientation one expects (a) a doublet of separation *ca.* 68 kHz with the field applied parallel to and (b) 136 kHz with the field applied perpendicular to the host layers. If the guest molecules adopt the parallel orientation, one expects (c) a powder spectrum if the molecules are statically disordered on the ^2H NMR time scale, (d) a doublet of separation *ca.* 34 kHz if the molecules undergo rapid C_2 reorientation with the field parallel to the layer planes, and (e) a doublet of separation ca. 68 kHz with the field perpendicular to the host layers.

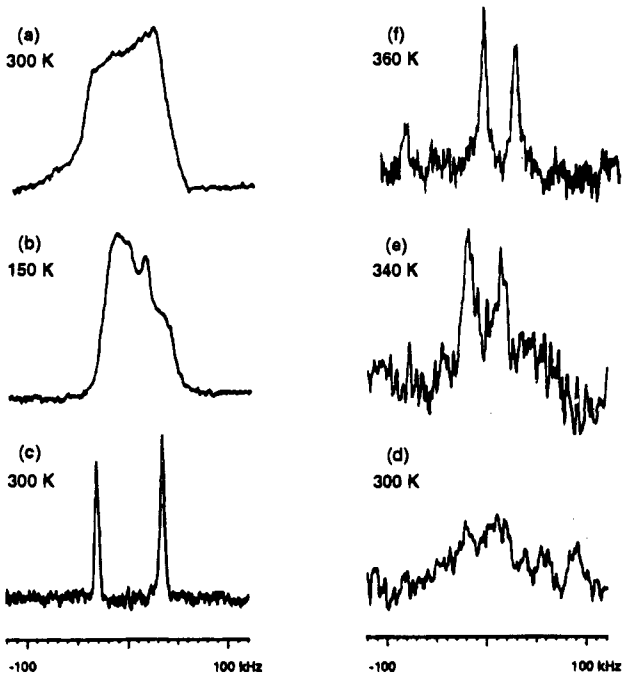

Figure 10. The static solid-state ^2H NMR spectra of powdered $Mn_{0.83}PS_3\{Co(Cp)_2\}_{0.34}(H_2O)_{0.3}$ at 300 K (a) and powdered $MnPS_3\{Co(Cp)_2\}_{0.34}(H_2O)_{0.3}$ at 150 K (b), a single crystal of $Mn_{0.83}PS_3\{Co(Cp)_2\}_{0.34}(H_2O)_{0.3}$ with its *c* axis parallel to the applied field at 300 K (c), and a single crystal of $MnPS_3\{Co(Cp)_2\}_{0.34}(H_2O)_{0.3}$ with its *c* axis perpendicular to the field at 300 (d), 340 (e), and 360 K (f).

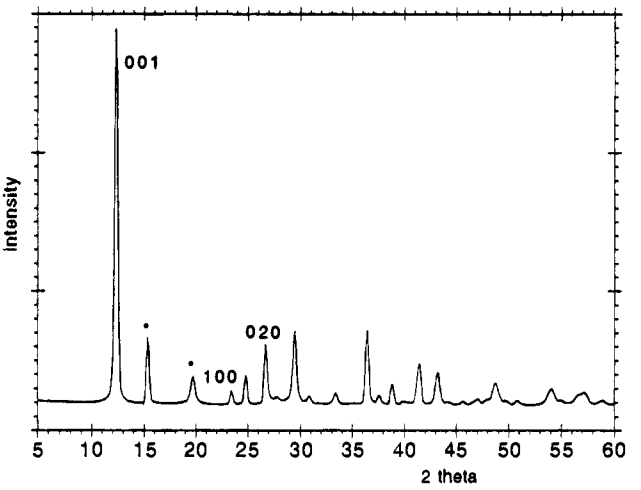

Figure 11. Powder neutron diffraction pattern of $Mn_{0.84}PS_3\{N(CD_3)_4\}_{0.32}(D_2O)_{0.9}$ recorded at 10 K. Superlattice reflections are marked with an asterisk. Wavelength 2.426 Å.

The results of both powder and single-crystal studies are shown in Figure 10. The unusual powder line shape and resulting lack of information is due to the presence of Mn^{2+} $S = {}^5/_2$ paramagnetic ions within the layers of the host lattice, which give rise to extreme local magnetic shifts and cause the deviation from the expected Pake Doublet line shape. From the single-crystal spectra, however, much information about the behavior of the guest molecules can be inferred. Firstly the spectrum with the applied field perpendicular to the host layers (Figure 10c) shows a separation of 66.89 kHz, indicating that the guest molecules adopt a single perpendicular orientation with respect to the external field and therefore an orientation with their principal molecular axes parallel to the layers of the host lattice. Spectra with the crystal layers oriented parallel to the applied field at a variety of temperatures between 300 and 360 K are shown in Figure 10, parts d–f. Despite the poor signal to noise of these spectra it can be seen that the spectral line shape evolves from a broad powder like pattern at room temperature to a sharp doublet of separation 33.2 kHz at higher temperatures, which indicates that the molecules are essentially static between the layers at room temperature but undergo a rotation around their C_2 axes at a rate which increases with temperature, approaching 10^8 Hz at 360 K.

Similar motional behavior has been recently discovered for other cobaltocene intercalates of layered sulfides[43] and has indicated that both guest–guest and guest–host interactions are of comparable importance in describing the packing arrangements in these host lattices.

2. Tetramethylammonium Intercalates of $MnPS_3$. (a) Powder Diffraction Studies. Powder X-ray and neutron diffraction patterns of $Mn_{0.84}PS_3\{NMe_4\}_{0.32}(H_2O)_{0.9}$ revealed it to be highly crystalline and considerably more ordered than the cobaltocene intercalate. The neutron diffraction pattern, recorded at 10 K, is shown in Figure 11. From this figure it can be seen that a series of sharp reflections are observed, and none of the broad "Warren" line shapes present in the neutron pattern of the cobaltocenium intercalate were apparent. It is also clear from Figure 11 that there are again reflections observed in the diffraction pattern which cannot be indexed on the basis of a unit cell directly related to that of $MnPS_3$. Low-angle superlattice reflections are marked with an asterisk in Figure 11. *hk*0 reflections were easily identified from the powder pattern by

Table 3. *hk*0 Reflections in the Powder Neutron Diffraction Pattern of $Mn_{0.84}PS_3\{NMe_4\}_{0.32}(H_2O)_{0.9}$[a]

$2\theta_{obs}$(deg)	d_{obs}/Å	*a b c*	*3a 2b c*	*6a 6a* ($\gamma = 120°$)
15.355	9.08	*	2 0 0	2 2 0
19.720	7.08	*	0 3 0	3 2 0
23.450	5.97	1 0 0	3 0 0	4 2 0
26.69	5.25	0 2 0	3 2 0	6 0 0
36.44	3.88	1 2 0	*	8 0 0
38.83	3.65	*	5 0 0	6 4 0
41.40	3.43	*	5 2 0	8 2 0

[a] Reflections are indexed on a variety of cells relate to that of pristine $MnPS_3$. Peaks which cannot be indexed on a given cell are represented by an asterisk.

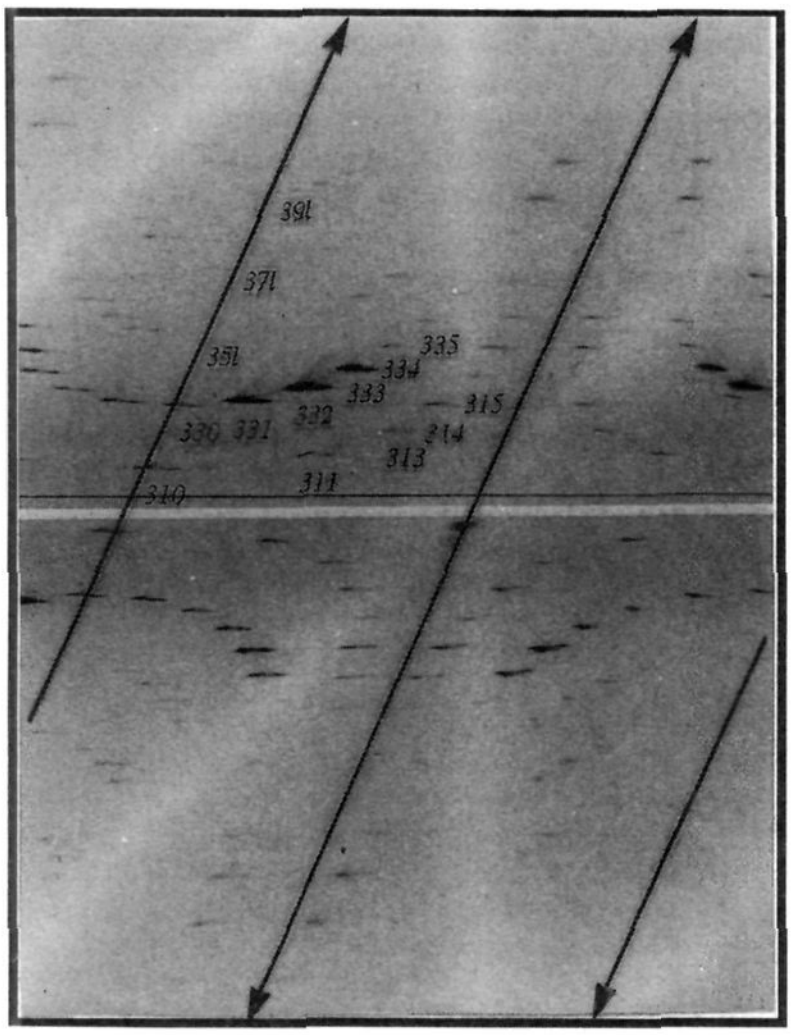

Figure 12. Single-crystal Weissenberg photograph of the $h = 3$ layer of $Mn_{0.84}PS_3\{NMe_4\}_{0.32}(H_2O)_{0.9}$. Order is seen on all $k = 2n$ lattice rows, in contrast to the cobaltocenium intercalate (Figure 5).

comparison with the spectrum of $Mn_{0.8}PS_3\{K\}_{0.4}(D_2O)_{1.0}$—which has similar *a* and *b* parameters, but a smaller *c* axis—and are reported in Table 3. It can be seen from these data that it is again necessary to adopt a unit cell which is considerably larger than that of the pristine host in the *a* and *b* directions in order to explain the observed diffraction pattern. This is again indicative of the formation of either a guest or vacancy superlattice in the intercalate and will be discussed below.

(b) Single-Crystal Studies on $Mn_{0.84}PS_3\{NMe_4\}_{0.32}(H_2O)_{0.9}$. Oscillation and Weissenberg photographs of a single crystal of $Mn_{0.84}PS_3\{NMe_4\}_{0.32}(H_20)_{0.9}$ were recorded. Oscillation photographs recorded with the crystal mounted along the *a* axis showed strong scattering from the $h = 0$, 1, and 2 reciprocal lattice layers, but again additional weak diffraction from intermediate layers corresponding to at least a tripling of the *a* axis was observed. Weissenberg photographs were recorded of the $h = 0$, 1/3, 2/3, 3/3, 4/3, 5/3, and *2* layers (corresponding to the $h = 0$, 1, 2, 3, 4, 5, 6 of the tripled cell). A typical photograph, that of the $h = 3$ layer, is shown in Figure 12.

It can be immediately seen from Figure 12 that the tetramethylammonium intercalate is considerably more ordered than the cobaltocenium intercalate. In particular discrete diffraction peaks are seen for all values of *k* in contrast to the cobaltocenium intercalate which shows diffuse scatter for layers except $k = 3n$. This effect can also be seen in the neutron diffraction pattern of Figure 11, where the 020 reflection of the tetramethylammonium intercalate is a sharp peak whereas that of the cobaltocenium intercalate was markedly broadened.

In order to describe the three-dimensional diffraction from this crystal it is therefore necessary to adopt a unit cell with *a* and *b* dimensions at least as large as those of the pristine host. Such cell dimensions then suggest that either Mn/P site ordering is retained on intercalation or the interlamellar guest species have a high degree of order.

Weissenberg photos of the intermediate layers revealed that while diffraction from these layers is weak (typical exposure times of 7 days being required) it was possible to record and index some 75 independent reflections from the $h = 1$, 2, and 4 layers. These reflections again showed a $h + k = 2n$ absence.

Attempts were again made to record the diffraction pattern of a single crystal of this sample using automated diffractometry techniques. The crystal of Figure 12 was transferred directly to an Enraf Nonius CAD-4 diffractometer and two strong independent reflections, identified from the Weissenberg photographs, and unit cell dimensions, known from powder diffraction studies, used to determine an orientation matrix. From this orientation matrix an additional 22 strong reflections were found and centered using a θ–2θ scan mode. These 24 reflections were then used to refine the unit cell parameters, giving a cell with $a = 6.10(1)$ Å, $b = 10.59(1)$ Å, $c = 11.53(1)$ Å, $\alpha = 90.2(1)°$, $\beta = 90.0(1)°$, $\gamma = 90.0(1)°$. The relative inaccuracy of this cell, as revealed by the magnitude of the standard deviations on unit cell dimensions and angles, is indicative of the difficulty in accurately centering the broad reflections from this class of material. For data collection a cell of *3a b c* was employed in the hope of recording intensity from the intermediate lattice layers observed on the oscillation photographs. A total of 5935 predicted reflections in the range $\theta < 58°$ were scanned, of which just 178 had $I > 3\sigma(I)$. All of these observed reflections had $h = 3n$, indicating that no meaningful diffraction data could be recorded from the intermediate layers. This again highlights the difficulty of recording reflections as broad as those of Figure 12 by simple ω–2θ scans; despite over 60 reflections being clearly visible on the zero level photograph alone, only 178 reflections were "observed" by the automated scan procedure. This paucity of intensity data and the extreme problems of absorption for plate-like samples, such as these, extremely restrict the structural information available.

It can, however, be seen from the unit cell parameters that intercalation has resulted in a change in the monoclinic angle, β, from 107.35° to 90°. One possible cause of this phenomenon is that the layer expansion which occurs upon intercalation of the guest ions is accompanied by a shift of the host lattice layers in the *a* direction by *a*/3. This process is analogous to a change from cubic to hexagonal close packing of the sulfur atoms and is shown schematically in Figure 13. There is some precedent for this type of a layer shift giving rise to changes in symmetry from both the observations made for the $Co(Cp)_2^+$ intercalate and the report of Lifshitz and co-workers of such a phase change occurring in pristine $CdPS_3$ at around 260 K,[53] where the symmetry change was accompanied by a *ca.* 2% reduction in the *c* axis dimension. Structural models based on such a layer shift were found to show excellent agreement between observed and calculated Patterson Functions, though further structural refinement proved impractical.

(53) Lifshitz, E.; Francis, A. H.; Clarke, R. *Solid State Commun.* **1983**, *45*, 273.

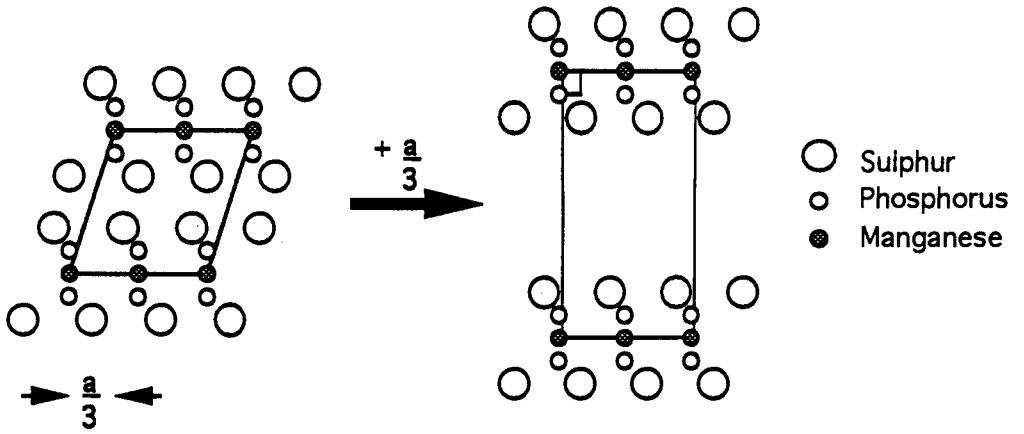

Figure 13. Schematic representation of how a layer shift of $a/3$ causes a change from a monoclinic cell with $\beta = 107.35°$ to a cell with $\beta = 90°$.

Discussion of the Structures

Origins of the Superlattice. There are a number of possible origins of the superlattice observed in the diffraction patterns of the two intercalates studied. One possibility is that it is caused by either a commensurate or an incommensurate packing of the guest molecules. A second possibility is that the metal vacancies which are formed during the intercalation process are arranged in an ordered manner within the host layers. If the cobaltocenium intercalate is considered first, then some insight into what causes the superlattice can be obtained. For this intercalate, the "superlattice reflections" are considerably stronger in the X-ray diffraction pattern (which is dominated by the atoms of the host layers) than in the neutron diffraction pattern (where scatter is dominated by the deuterated guest molecule). It therefore seems unlikely that solely a superlattice of guest molecules could give rise to the effects observed. It is therefore reasonable to conclude that an ordered array of intralayer metal vacancies gives rise to the observed superlattice. This is further supported by the observation of significantly broadened $hk0$ reflections in the neutron diffraction pattern, which indicates some disorder in the guest packing, whereas the X-ray superlattice reflections are sharp peaks.

In the case of the tetramethylammonium intercalate, however, superlattice reflections are strong in both the neutron and X-ray patterns, and are sharp in both. This suggests that there is both an ordered array of metal vacancies within the layers **and** an ordered array of interlayer guest species. The implications of such a scheme are discussed further below.

Further support that an ordered array of metal vacancies can give rise to observable effects in the diffraction pattern of these materials comes from the related compound $In_{2/3}PS_3$, which adopts a structure very similar to that of $MnPS_3$, but in which one-third of the possible metal sites are vacant. In this compound preliminary evidence indicated that the unit cell was tripled in the a direction, though no full crystal structure was reported.[54] Studies on the analogous $In_{2/3}PSe_3$, however, showed no evidence for any superlattice.[55]

Finally, investigations on the magnetic scattering of these lattices, which will be reported in full elsewhere,[56] have revealed that the superlattice reflections have significant magnetic contributions to their intensity below T_C (*ca.* 40 K), showing that the superlattice and magnetic properties of these materials (which are dominated by the layer Mn^{2+} $S = {}^5/_2$ ions) are intimately related.

(54) Soled, S.; Wold, A. *Mater. Res. Bull.* **1976**, *11*, 657.
(55) Katty, A.; Soled, S.; Wold, A. *Mater. Res. Bull.* **1977**, *12*, 663.
(56) Evans, J. S. O.; O'Hare, D.; Clement, R. Manuscript in preparation.

Comparison of the Structures. The structures of the two intercalation compounds studied, while being broadly similar, do show a number of important differences in their detail, despite both compounds having essentially the same chemical formula, $Mn_{0.83}PS_3\{guest\}_{0.33}(solvent)_y$. Perhaps the most important of these features is the retention of Mn/P site ordering in the tetramethylammonium intercalate as opposed to its loss in the cobaltocenium.

One possible reason for this difference in structure can be seen by considering the different shapes of the two guest molecules. In the case of the cobaltocene intercalate, the overall crystal structure could be described in terms of a structure in which layer shifts occur in the ab plane such that sulfur atoms in adjacent layers lie directly above and below one another.

The van der Waals surface of the tetramethylammonium molecule, however, is essentially spherical in nature, and as such the guest molecule may prefer to adopt an octahedral site between the host layers. A layer shift of $a/3$ on intercalation would give rise to both the orthorhombic cell observed and six such octahedral sites per unit cell—the overall cell contents being $Mn_4P_4S_{12}(Oh\ site)_6$. From the stoichiometry of the intercalate of $Mn_{5/6}PS_3\{guest\}_{1/3}$ it is clear that not all these octahedral sites can be filled at any given time; simple calculations indicate that only two in every nine of the available octahedral sites will be occupied. To give the experimentally observed guest: PS_3 ratio, it is necessary to adopt a cell which contains one guest molecule for every three phosphorus atoms present. One possible such cell, which actually contains 2 guest molecules and 6 phosphorus atoms, has dimensions $a = 18.3$ Å, $b = 6.1$ Å, and $\gamma = 120°$ and is shown in Figure 14a.

It is then possible to build a structural model which incorporates both an ordered system of metal vacancies **and** a commensurate ordered array of guest molecules. Since the stoichiometry of the material indicates a metal vacancy of 1 site in 6, the unit cell describing these vacancies must contain a minimum of 6 original metal sites. This necessitates the adoption of a unit cell larger than that describing the pristine layers, and one such possible ordering scheme is shown in Figure 14a, where the vacancy ordering adopted gives rise to a cell with dimensions $a = b = 10.59$ Å and $\gamma = 120°$.

It can be seen that these two superlattice cells are related to each other, and that to describe the ordering of both the guest molecules and the metal vacancies simultaneously one must adopt a much larger cell with $a = b = 36.6$ Å and $\gamma = 120°$. The overall contents of a single layer in the repeat unit will then be $Mn_{60}P_{72}S_{216}\{guest\}_{24}$, which simplifies to the observed $Mn_{0.83}PS_3\{guest\}_{0.33}$. Similar structural arguments will apply to the cobaltocenium intercalate, although here the actual sites

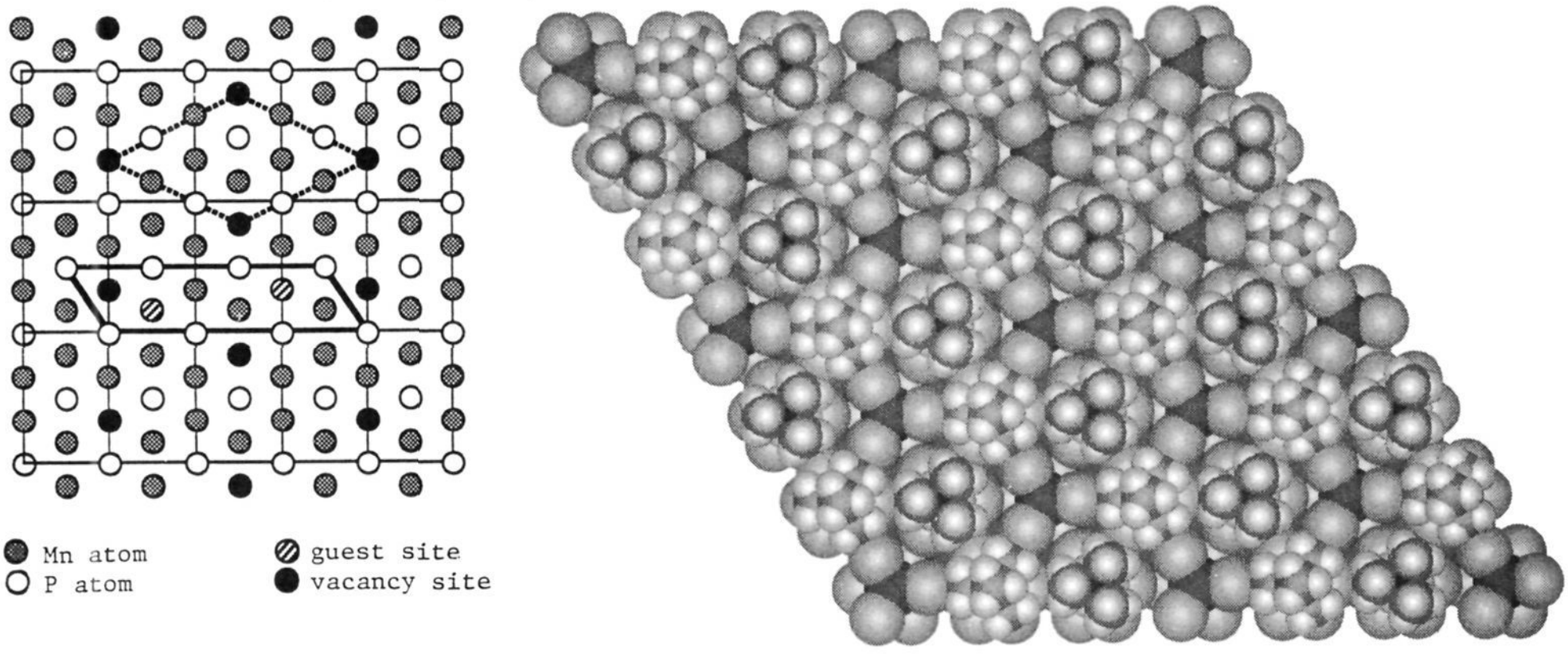

Figure 14. (a, left) Possible vacancy and guest super lattices: a solid line represents a possible arrangement of ordered guest molecules; a dashed line represents a possible vacancy cell. Only the proposed octahedral guest sites within one unit cell are depicted for clarity. (b, right) The arrangement of NMe_4^+ cations in $Mn_{0.84}PS_3\{NMe_4\}_{0.32}(H_2O)_{0.9}$ viewed perpendicular to the host layers. The combination of guest and vacancy cells requires a much larger overall cell; $Mn_{0.84}PS_3\{NMe_4\}_{0.32}(H_2O)_{0.9}$ requires an overall cell of $a = b = 18.3$ Å and $\gamma = 120°$.

adopted by the guest molecules will be different. An overall view of one possible structure is shown in Figure 14b.

Conclusions. These studies have shown that in order to fully understand the structure of molecular intercalates such as these it is necessary to employ a range of complementary structural techniques—X-ray diffraction being particularly suited to study of the host layers and neutron diffraction and NMR techniques being required to study the guest molecules. A combination of the above techniques has revealed that these intercalates retain a remarkable degree of long-range order within the host lattice layers, requiring the adoption of unit cells considerably expanded in the a and b dimensions. The variety of possible stacking sequences along the c axis, however, can lead to a structure which has considerable 3-dimensional disorder. The direct observation of a metal vacancy superstructure for the first time has led to a good understanding of the origins of the spontaneous magnetization of these materials, which will be discussed elsewhere, and has also suggested a model whereby the ordering of NLO chromophores in the $DAMS^+$ intercalate can be explained.

Acknowledgment. The authors thank Pierre Thuéry of the Léon Brillouin Laboratory, Saclay, Paris for his assistance in recording the neutron diffraction data and Dr. Susan Mason for assistance with the solid-state NMR experiments. We also thank the SERC and the British Council Alliance Scheme for support.

JA9429733